A flexible and scalable scheme for mixing computed formation energies from different levels of theory

Ryan Kingsbury,[1,2] Andrew S. Rosen,[1,3] Ayush S. Gupta,[1] Jason Munro,[3] Shyue Ping Ong,[4,3] Anubhav Jain,[2] Shyam Dwaraknath,[3] Matthew Horton,[3] and Kristin A. Persson[1,5,*]

[1] *Department of Materials Science and Engineering, University of California Berkeley, Berkeley, CA 94720*
[2] *Energy Technologies Area Lawrence Berkeley National Laboratory, Berkeley, CA 94720*
[3] *Materials Science Division Lawrence Berkeley National Laboratory, Berkeley, CA 94720*
[4] *University of California San Diego, La Jolla, CA 92093*
[5] *Molecular Foundry Lawrence Berkeley National Laboratory, Berkeley, CA 94720*

(Dated: March 3, 2022)

Phase stability predictions are central to computational materials discovery efforts and have been made possible by large databases of computed properties from high-throughput density functional theory (DFT) calculations. Such databases now contain millions of calculations at the generalized gradient approximation (GGA) level of theory, representing an enormous investment of computational resources. Although it is now feasible to carry out large numbers of calculations using more accurate methods, such as meta-GGA functionals, recomputing the entirety of a database with a higher-fidelity method is impractical and would not effectively leverage the value embodied in existing calculations. Instead, we propose in this work a general procedure by which higher-fidelity, low-coverage calculations (e.g., meta-GGA calculations for selected chemical systems) can be combined with lower-fidelity, high-coverage calculations (e.g., an existing database of GGA calculations) in a robust and scalable manner to yield improved phase stability predictions. We demonstrate our scheme using legacy GGA($+U$) calculations and new r^{2}SCAN meta-GGA calculations from the Materials Project and illustrate its application to solid and aqueous phase stability. We discuss practical considerations for constructing mixed phase diagrams and present guidelines for prioritizing high-fidelity calculations for maximum benefit.

I. INTRODUCTION

The advent of large databases of computed material properties, such as the Materials Project [1], AFLOW [2], the Open Quantum Materials Database (OQMD) [3, 4], and the Joint Automated Repository for Various Integrated Simulations (JARVIS) [5], has paved the way for a new era of data-driven materials science [6]. These databases now contain computed properties derived from millions of individual calculations, the vast majority of which employ density functional theory (DFT) due to its efficient compromise between computational cost and accuracy. For example, the Materials Project [1] contains computed formation energies for more than 140,000 materials calculated using the Perdew–Burke–Ernzerhof (PBE) [7] generalized gradient approximation (GGA) [8] functional, with a Hubbard U value [9] and empirical energy corrections [10] applied to some chemical systems. This data is widely used in machine learning and computational materials screening efforts in which the thermodynamic (meta)stablility of a material is often among the first selection criteria [11].

Despite its versatility and historical success, PBE has well-documented systematic errors related to electron self-interaction [12, 13] that are particularly notable in diatomic gases [14, 15] and transition metal compounds with localized electronic states [1, 15, 16]. PBE also fails to capture medium- and long-range dispersion interactions [17], which are important for describing the properties of weakly-bound systems. Even when adjusted using empirical correction schemes, the mean absolute error (MAE) in formation energies predicted by this level of theory are still on the order of 50–200 meV/atom [10, 14, 15, 18–22], although the error in energy differences among polymorphs is typically lower (e.g. 25 meV/atom) [23].

Today, more than a decade after most materials databases were established [6], theoretical advances and growth in computing power have made it feasible to compute large numbers of formation energies at higher levels of theory [18], which could substantially increase their accuracy. For example, we recently showed that the restored-regularized Strongly Constrained and Appropriately Normed (r^{2}SCAN) meta-GGA functional [24] reduced the error in predicted formation energies of strongly-bound and weakly-bound materials by 50% and 15%, respectively, compared to the PBEsol [25] GGA functional, while simultaneously exhibiting reliable convergence [18]. The original SCAN functional [26] on which it is based has also been shown to predict volumes, lattice constants, and ground-state structures of

* kapersson@lbl.gov; https://materialsproject.org/

many materials more accurately than PBE [22, 27–31].

Carrying out enough higher-fidelity calculations to comprehensively cover technologically-relevant chemical spaces, as is required for the construction of compositional phase diagrams and the discovery of new structure–property relationships, could clearly benefit the many materials discovery efforts that depend on such data. However, replacing *all* of the existing lower-fidelity (GGA) calculations in large materials databases with higher-fidelity (e.g., meta-GGA) calculations would consume an enormous amount of energy and computing time, since SCAN and r^{2}SCAN, for example, have 4–5× the computational cost of PBE [18, 22, 32]. Even if resources were unlimited, there is likely to be little benefit in recomputing materials that are highly unstable (i.e., far from the convex energy hull), since predicting (meta)stability is of primary importance. Furthermore, meta-GGA calculations will not improve formation energy predictions to an equal extent for all materials. For example, SCAN has been shown to be slightly *less* accurate than PBE in predicting the formation energies of weakly-bound materials (e.g., intermetallics [22]), and r^{2}SCAN improves the predictions for these materials to a much lesser extent than for strongly-bound materials [18].

Therefore, instead of recomputing materials *en masse*, higher-fidelity calculations should be targeted at the materials for which they are likely to improve the accuracy of the phase diagrams the most (e.g., strongly-bound materials, materials close to the energy convex hull). Adopting this strategy will economize future use of resources and preserve the massive investment embodied in existing lower-fidelity calculations. Notably, however, such an approach will require phase stability predictions to be based on a mixture of formation energies computed at different levels of theory. The most straightforward way to systematically improve upon GGA phase diagrams in a high-throughput manner, which we refer to here as "naive mixing", is simply to build each phase diagram using formation energies from lower level calculations, and then replace them with higher level calculations whenever they are available. However as we will show, constructing mixed phase diagrams this way can result in severe distortions to the shape of the convex energy hull and dramatically worsen phase stability predictions.

As an alternative to naive mixing, we propose in this work a scheme to construct phase diagrams that mix calculations from different density functionals comprising a lower-fidelity, higher coverage and a higher-fidelity, lower coverage set of calculations (here, PBE($+U$) and r^{2}SCAN) with minimal risk of distortion. By defining the reference state at each point in compositional space as the ground state PBE($+U$) structure, we build a framework in which energies from any two functionals can be mixed in a robust and scalable manner that preserves the shape of the convex hull. After presenting our mixing scheme, we assess how a transition from PBE($+U$) to r^{2}SCAN affects predicted polymorph stability and energy above hull by analyzing a set of approximately 33,900 r^{2}SCAN calculations and discuss strategies for prioritizing r^{2}SCAN calculations such that the mixed phase diagram most closely approximates the full r^{2}SCAN phase diagram. We conclude by using our mixing scheme to analyze solid and aqueous phase stability in two example systems. The mixed phase diagrams presented in this work, along with the 33,000+ new r^{2}SCAN calculations, are made publicly available in the Materials Project database [1] to increase the accuracy of future computational material science efforts.

II. THEORETICAL FRAMEWORK FOR MIXING FORMATION ENERGIES FROM DIFFERENT FUNCTIONALS

A. Mixing rules

The computed energy of formation for a material, ΔH_f, is defined with respect to the elements by [9, 19, 21, 33]

$$\Delta H_f^{298\text{K,DFT}} \approx E^{0\text{K,DFT}} - \sum_{\text{el}} n_{\text{el}} E_{\text{el}}^{0\text{K,DFT}} \qquad (1)$$

where $E^{0\text{K,DFT}}$ is the total electronic energy computed from DFT at 0 K, subscript 'el' represents each of the constituent elements in the material, and n are stoichiometric coefficients. We note that E can include empirical corrections and that this formulation assumes that differences in finite-temperature enthalpy between materials are negligible. Electronic energies E are not intrinsically meaningful, and their energy scales differ substantially among functionals for the same material. However, the *differences* in electronic energy among materials and elements, and hence the value of ΔH_f, define a consistent, physically-meaningful quantity that can be compared among different levels of theory.

In this manuscript, we consider mixing GGA($+U$) and r^{2}SCAN calculations; although the scheme we present here can be used to mix energies from any two functionals. Note that we use "GGA($+U$)" to refer to the mixture of empirically-corrected PBE and PBE+U calculations that currently populate the Materials Project Database. Specifically, the Materials Project uses PBE (i.e., GGA) for all materials except those containing `Co`, `Cr`, `Fe`, `Mn`, `Mo`, `Ni`, `V` and `W`, which are calculated with a Hubbard U value [34]. These GGA and GGA+U calculations are combined using the mixing scheme of Jain et al. [9] to yield a consistent set of formation energies. In this work, we use this combination of adjusted GGA and GGA+U calculations as our high-coverage, low-fidelity set of calculations, while "r^{2}SCAN" denotes unadjusted meta-GGA energies that comprise the low-coverage, higher-fidelity calculations. Additional details regarding the computational methods for each calculation type are provided in Section V.

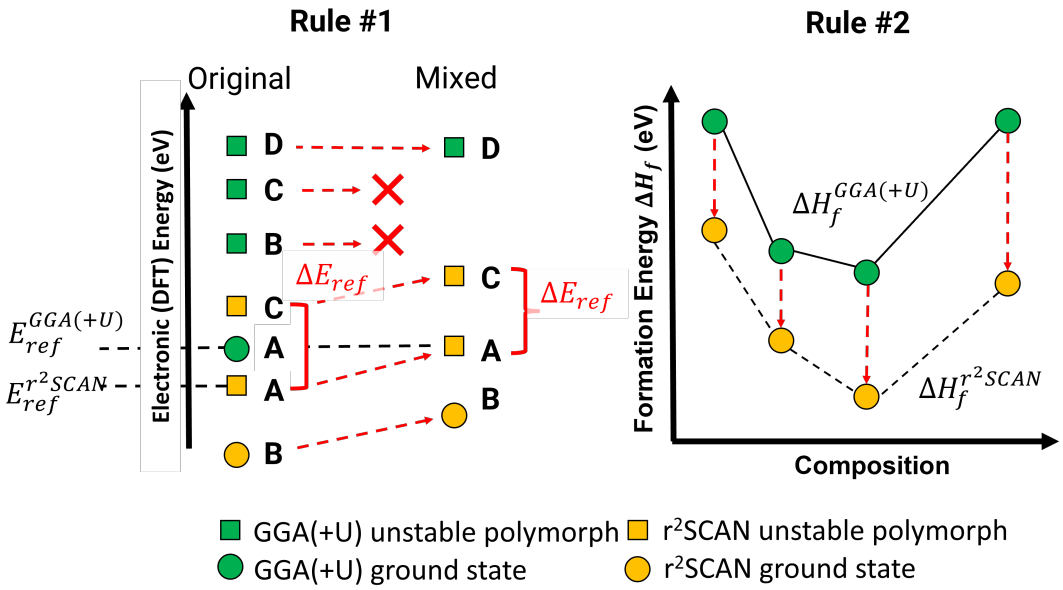

FIG. 1. Rules for mixing GGA($+U$) (green) and r^{2}SCAN (yellow) energies onto a single phase diagram. 1) r^{2}SCAN energies can be placed onto a GGA($+U$) hull by referencing them to the r^{2}SCAN energy of the GGA($+U$) ground state via ΔE_{ref}. In the diagram, A, B, C, and D represent different polymorphs at a single composition, and polymorph A is the GGA($+U$) ground state. E_{ref}^{GGA+U} and $E_{ref}^{r^2SCAN}$ are the electronic (DFT) energies of polymorph A in the two functionals. GGA($+U$) energies of polymorphs that also exist in r^{2}SCAN (e.g., polymorphs B and C) are removed. 2) The convex hull is built with r^{2}SCAN formation energies only when there are r^{2}SCAN calculations for every GGA($+U$) ground state.

As noted in the Introduction, the most straightforward approach to constructing mixed r^{2}SCAN / GGA($+U$) phase diagrams is "naive mixing", where we simply replace GGA($+U$) formation energies with r^{2}SCAN formation energies whenever r^{2}SCAN calculations are available, while using GGA($+U$) formation energies everywhere else. There are two drawbacks with naive mixing. First, in chemical systems where r^{2}SCAN predicts significantly smaller or larger formation energies than GGA($+U$) for most compounds, inserting a single r^{2}SCAN formation energy onto a GGA($+U$) phase diagram can either cause that single phase to move off the hull (if $\Delta H_f^{\text{r}^2\text{SCAN}} \gg \Delta H_f^{\text{GGA}(+U)}$), or cause adjacent phases to disappear from the hull (if $\Delta H_f^{\text{r}^2\text{SCAN}} \ll \Delta H_f^{\text{GGA}(+U)}$), when neither would occur on a full r^{2}SCAN phase diagram. Second, in many cases r^{2}SCAN stabilizes a different ground-state structure for the elements than GGA($+U$) (see Appendix B). Naive mixing of formation energies in chemical systems containing one of these elements is not rigorously consistent, because the formation energies are being referenced to different structures.

To circumvent these issues, we build our mixing scheme by considering all formation energies to be the sum of a reference energy and a relative energy. We define the reference energy, E_{ref}, for each functional as *the formation energy of the GGA(+U) ground state structure at each point in compositional space*, where the formation energy is calculated with respect to elemental endpoints relaxed with that functional. The energy of any material in either functional may then be expressed as a difference, ΔE_{ref}, relative to the corresponding reference energy. Note that ΔE_{ref} is calculated directly from the difference in polymorph energies, and hence does not depend on the energies of the elemental endpoints. Our mixing scheme is similar in spirit to the previous GGA/GGA+U mixing scheme as well as the combined computational-experimental Pourbaix diagrams of the Materials Project [9, 35]; however extends these approaches to be applicable to any two functionals without relying on pre-fitted energy correction parameters.

Using this framework, we propose two "mixing rules" that define our scheme for constructing mixed r^{2}SCAN / GGA($+U$) phase diagrams. These mixing rules are summarized schematically in Figure 1 and briefly elaborated below. In sections that follow, we will illustrate each rule with an example.

1. Beginning with a GGA($+U$) hull, replace GGA($+U$) energies with r^{2}SCAN energies by adding their ΔE_{ref} to the corresponding GGA($+U$) reference energy.

2. Construct the convex energy hull using $\Delta H_f^{\text{r}^2\text{SCAN}}$ only when there are r^{2}SCAN calculations corresponding to every reference structure (every GGA($+U$) stable structure). In this case, add any missing GGA($+U$) materials by adding their ΔE_{ref} to the corresponding r^{2}SCAN reference energy.

Rule #1 provides a means to introduce r^{2}SCAN energies onto GGA(+U) phase diagrams when r^{2}SCAN calculations are only available for one or a few compositions. In Figure 1, polymorph A represents the reference structure (GGA(+U) ground state). Since the reference structure is, by definition, on the GGA(+U) hull, the r^{2}SCAN relaxed structure corresponding to this reference structure (as determined by the PYMATGEN [36] `StructureMatcher` algorithm) is assigned $\Delta H_f^{\mathrm{GGA}(+U)}$. Polymorphs B and C, calculated in r^{2}SCAN, are assigned energies that maintain their energy difference with respect to the reference structure, ΔE_{ref}. For example, if polymorph C is 10 meV/atom higher in energy than polymorph A in r^{2}SCAN, it would be assigned an energy $\Delta H_f^{\mathrm{GGA}(+U)}$ + 10 meV/atom. It is also possible for this method to place a polymorph below the GGA(+U) hull. Polymorph B is unstable with respect to the reference structure in GGA(+U) but is lower in energy than the reference structure in r^2. If it were 10 meV/atom lower than the reference structure in r^{2}SCAN, it would be assigned an energy $\Delta H_f^{\mathrm{GGA}(+U)} - 10$ meV/atom, slightly changing the shape of the hull in the mixed phase diagram compared to GGA. Finally, polymorphs that do not have a r^{2}SCAN energy (such as polymorph D) maintain their energy with respect to the GGA(+U) hull.

When r^{2}SCAN calculations become available for every reference state, then, by Rule #2, the convex hull is computed directly with r^{2}SCAN formation energies ($\Delta H_f^{\mathrm{r^2SCAN}}$). Now, any unstable GGA(+U) phases that have not been calculated in r^{2}SCAN can be added to the diagram by adding their ΔE_{ref} to the $H_f^{\mathrm{r^2SCAN}}$ of the corresponding reference structure. In other words, we invert Rule #1 so that r^{2}SCAN structures become the reference structures.

Note that a central assumption of our mixing scheme is that r^{2}SCAN energies are always preferable to GGA(+U) energies. This assumption is well-justified by the generally superior accuracy of SCAN and r^{2}SCAN formation energies reported in many studies [18, 22, 27–31]. In general, application of our mixing scheme should be restricted to pairs of functionals where one has an *a priori* reason to prefer one energy over another. In addition, we note that in principle it is possible to use our framework to mix energies from more than two functionals, provided that reference energies are available within each functional and that a clear hierarchy can be established among them.

B. Mixed diagrams for relative polymorph stability (Rule #1)

We illustrate the motivation behind Rules #1 and 2 using the Sn–Br phase diagram, which is shown in Figure 2. In general, when constructing phase diagrams we seek to determine 1) the shape of the convex energy hull (i.e., stable compositions and their formation energies), and 2) the stable polymorph at each composition. Figure 2a and 2b compare the Sn–Br phase diagram with the formation energy of all phases calculated in GGA(+U) and r^{2}SCAN, respectively, and show that the accuracy of both aspects is improved by r^{2}SCAN. GGA(+U) incorrectly predicts the ground-state polymorph of $SnBr_2$ as rocksalt (spacegroup $P\bar{3}m1$) and overpredicts the magnitude of ΔH_f as -1.136 eV/atom, whereas the experimental value is estimated at -0.84 - 0.92 eV/atom [37] (indicated by the shaded band in Figure 2). By contrast, r^{2}SCAN correctly predicts the $SnBr_2$ ground state as *Pnma* [28] and makes a substantially more accurate prediction of its formation energy (-0.833 eV/atom).

As we have discussed, it is not always feasible to recompute an entire chemical system using r^{2}SCAN (as we have done to construct Figure 2b). When improving predictions of polymorph stability is a primary research objective, it makes sense to prioritize r^{2}SCAN calculations for all known polymorphs at the composition of interest. However, if we were to apply this strategy to $SnBr_2$ and replace all GGA(+U) formation energies of $SnBr_2$ polymorphs with r^{2}SCAN energies using naive mixing (Figure 2c), $SnBr_2$ would no longer be predicted as stable. This occurs because the entire hull is shallower (smaller magnitude of ΔH_f) in r^{2}SCAN than in GGA(+U), and hence using an r^{2}SCAN formation energy for $SnBr_2$ causes it to move off the hull. Instead, we must apply Rule #1 to make the r^{2}SCAN energies compatible with the GGA(+U) hull. We do so by positioning r^{2}SCAN formation energies relative to the GGA(+U) ground state polymorph ($P\bar{3}m1$), as shown in Figure 2d. Because we maintain the energy differences relative to this reference energy, the correct polymorph is now stabilized.

Compared to naive mixing of formation energies, applying Rule #1 preserves the overall shape of the GGA(+U) convex hull while enabling improvement in phase stability predictions using as few as two r^{2}SCAN calculations (one for the polymorph of interest and one for the reference structure). However, because r^{2}SCAN stabilizes the *Pnma* polymorph instead of the $P\bar{3}m1$ polymorph stabilized by GGA(+U), ΔH_f is lowered (and made less accurate) by 37 meV/atom, which is the difference in energy between the $P\bar{3}m1$ and *Pnma* polymorphs in r^{2}SCAN. Hence, although use of Rule #1 for study of a single composition may yield more accurate relative polymorph energies, it carries the risk of making the magnitude of the formation energy slightly less accurate compared to a full r^{2}SCAN phase diagram.

C. Mixed diagrams for formation energy (Rule #2)

When identifying stable compositions or predicting accurate formation energies is the primary research objective, it makes sense to prioritize recomputing all GGA(+U) ground states in r^{2}SCAN, as shown in Figure 2e. Applying Rule #2, this strategy allows the entire

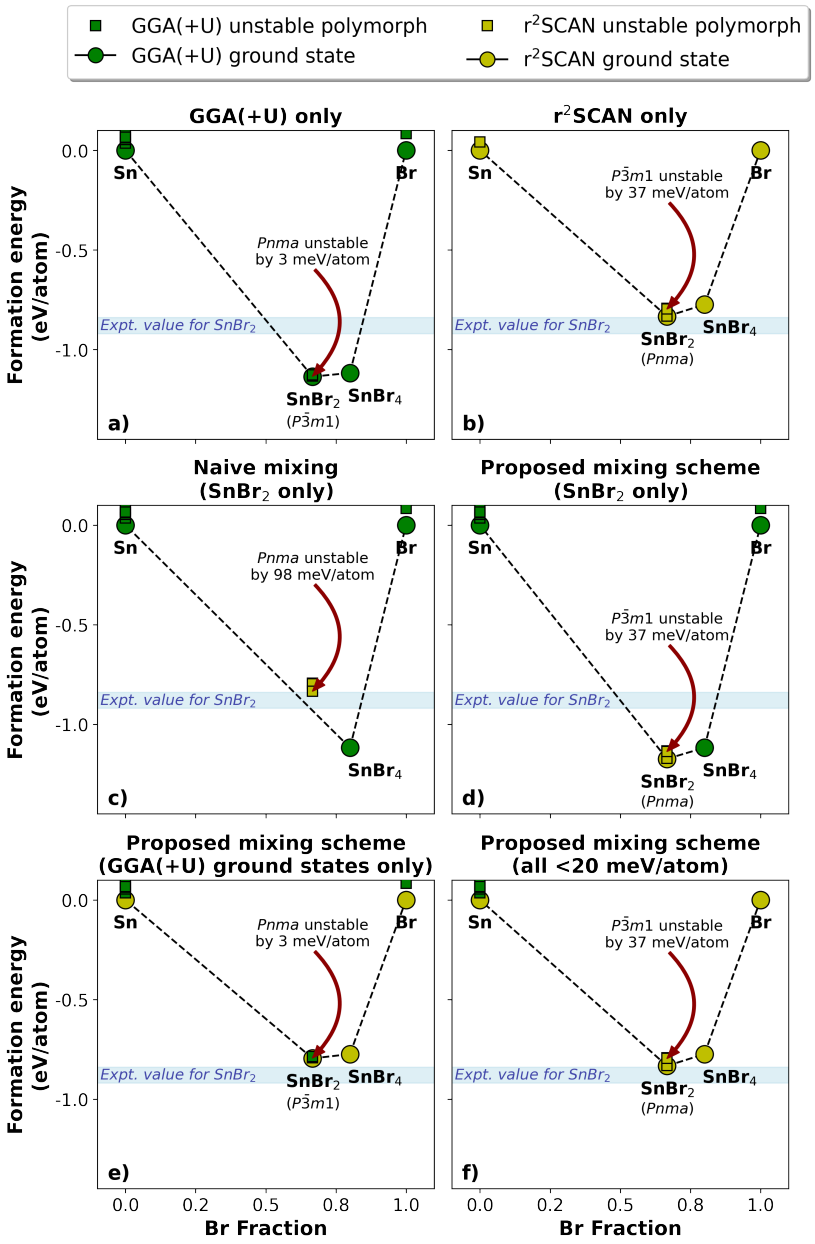

FIG. 2. Sn–Br phase diagram constructed using different mixing strategies for GGA($+U$) and r^{2}SCAN calculations. a) GGA($+U$) only; b) r^{2}SCAN only; c) naive mixing of formation energies, where all $SnBr_2$ polymorphs are computed in r^{2}SCAN and all other materials are in GGA; d) the same set of energies as c), but employing our mixing scheme (Rule #2); e) r^{2}SCAN for all reference states (i.e., GGA($+U$) ground states) and GGA($+U$) for all other materials; f) r^{2}SCAN for all materials within 20 meV/atom of the GGA($+U$) convex hull. The numerical value in parentheses indicates the energy above hull of the experimental ground state *Pnma* polymorph of $SnBr_2$. The shaded blue regions represent the estimated range of experimental formation energies for $SnBr_2$ [37]. Tabulated r^{2}SCAN and GGA($+U$) energies for all materials are provided in Appendix E.

convex hull to be constructed using $\Delta H_f^{\mathrm{r^2SCAN}}$. Unstable GGA($+U$) polymorphs are then positioned relative to the corresponding reference structures. Several unstable polymorphs of Sn that were mixed in this manner are visible in Figure 2e.

In this chemical system, recomputing the hull when only the GGA($+U$) ground states have been calculated in r^{2}SCAN will still not recover the exact r^{2}SCAN formation energy for $SnBr_2$, because GGA($+U$) stabilizes the incorrect ground state, and Rule #2 treats this incorrect ground state as the reference energy. Hence, the formation energy of $SnBr_2$ predicted by the mixed phase diagram in Figure 2e is too high by 37 meV/atom (the difference in energy between the $P\bar{3}m1$ and *Pnma* polymorphs in r^{2}SCAN).

Because there is no way to know *a priori* whether

r^{2}SCAN will stabilize a different ground state than GGA($+U$), a more robust strategy is to compute all polymorphs within some tolerance of the GGA($+U$) hull. Computing both ground states and slightly metastable polymorphs with r^{2}SCAN makes it more likely that the shape of the convex energy hull in the mixed phase diagram will be identical to that in a full r^{2}SCAN diagram. We apply this strategy in Figure 2f, in which we mix r^{2}SCAN energies for all materials within 20 meV/atom of the GGA($+U$) hull, and use GGA($+U$) energies for all other materials. The value of 20 meV/atom is motivated by analysis presented later (see Section III B) indicating that materials with higher $\Delta E_{\text{hull}}^{\text{GGA}(+U)}$ are rarely stabilized by r^{2}SCAN. With this strategy, the shape of the resulting energy hull (Figure 2f) exactly matches that of the pure r^{2}SCAN hull (Figure 2b).

Comparing Figures 2a, 2c, and 2e illustrates the importance of Rule #2 when mixing r^{2}SCAN and GGA($+U$) calculations. Formation energies cannot be naively mixed without carrying a substantial risk of over- or understabilizing certain compositions. The hull must remain in GGA($+U$) until there are r^{2}SCAN calculation corresponding to every reference state. Even in that case, it is preferable to include slightly unstable polymorphs in order to achieve better accuracy in cases where r^{2}SCAN stabilizes different polymorphs.

III. PRACTICAL CONSIDERATIONS

A. Mixed diagrams for ternary and higher systems

Ternary or higher-dimensional chemical spaces present special challenges for mixing energies between functionals, because strict application of mixing rules #1 and #2 can introduce inconsistencies between the full phase diagrams and those of constituent subsystems. For example, consider a case in which all of the GGA($+U$) ground states in chemical system A–B are computed in r^{2}SCAN. According to Rule #2, the binary A–B phase diagram would be constructed using $\Delta H_f^{\text{r}^2\text{SCAN}}$. This may result in different formation energies and/or predicted stable phases than the GGA($+U$) phase diagram, as illustrated previously for the Sn–Br system. Now suppose that we wish to construct a ternary phase diagram for the A–B–C system, in which there are multiple ternary ground states that have not been computed in r^{2}SCAN. Since the A–B–C system does not satisfy the requirements for Rule #2, we would construct this ternary phase diagram using $\Delta H_f^{\text{GGA}(+U)}$. This could result in the ternary A–B–C diagram predicting different formation energies and/or stable phases in the A–B subsystem than the binary A–B diagram. Such an inconsistency may be problematic depending on the use case. Note that if all reference energies in the full A–B–C system have been recomputed in r^{2}SCAN, then strict application of the mixing rules will not result in any inconsistencies. However, due to the much larger number of ternary and higher materials (compared to binaries), it becomes progressively more difficult to recompute all the reference energies needed to apply Rule #2 as the size of the chemical system increases.

In cases where consistency between lower- and higher-dimension phase diagrams is essential, one may apply the mixing rules individually to each chemical subsystem, in order of increasing dimensionality. To continue the example above, Rule #1 and Rule #2 would be applied individually to each of the A–B, B–C, and A–C chemical systems. The ternary phase diagram would then be constructed by combining these pre-adjusted binary formation energies with GGA($+U$) formation energies. An example of such a diagram is presented in Figure C.2.

Applying the mixing scheme to binary subsystems before treating the ternary system amounts to a modified form of naive mixing because it involves directly combining formation energies obtained from GGA($+U$) (for ternaries) with those calculated with r^{2}SCAN for binaries, without considering whether r^{2}SCAN energies are available for all ternary ground states. As such, mixed phase diagrams for high-dimensional chemical systems that are constructed in this manner should be used sparingly and interpreted with care. However, due to the inherently larger number of phases involved in higher dimensional systems, we expect this modified form of naive mixing to be less likely to cause severe distortions of the hull compared to binary systems.

To test this hypothesis, we compared ternary phase stability predictions from approximately 6,000 ternary phase diagrams computed in GGA($+U$) to mixed versions constructed using $\Delta H_f^{\text{r}^2\text{SCAN}}$ values for all binary subsystems and $\Delta H_f^{\text{GGA}(+U)}$ for all ternary materials (see Appendix C). We evaluated how frequently these "edged" diagrams either 1) destabilized a known experimental ternary phase (i.e., a phase reported in the Inorganic Crystal Structure Database [38]) that was stable in pure GGA($+U$) or 2) stabilized a known experimental ternary phase that was unstable in pure GGA($+U$). For the majority of chemical systems (83%), experimental ternary materials predicted stable by the pure GGA($+U$) diagram remained so in the mixed phase diagram, while in another 14% of cases exactly one material was destabilized. Similarly, for 94% of chemical systems, experimental materials predicted unstable by the pure GGA($+U$) diagram remain so in the mixed diagram, while for 6% of chemical systems exactly one unstable experimental material was stabilized (see Figure C.1). Thus, although employing modified naive mixing (i.e., "edged" phase diagrams) to achieve consistency between lower- and higher-dimensional phase diagrams carries a modest risk of destabilizing known experimental phases for some chemical systems, there are many other cases in which the mixed diagrams stabilize experimental phases that pure GGA($+U$) does not. Altogether, these results suggest that modified naive mixing is unlikely to *severely*

distort phase stability predictions.

B. Definition of materials "close to the hull"

In Section II we observed that it is preferable to recompute not just GGA(+U) ground states, but also materials close to the convex energy hull in order to ensure that the mixed energy hull has the correct shape (compare Figures 2e and f). This begs the question of how to define "close to the hull". More specifically, we can rephrase the question as "how likely is r^{2}SCAN to stabilize a material that is X meV/atom above the hull in GGA(+U)?" For example, a material that is 500 meV/atom above hull in GGA(+U) will almost certainly not become stable in r^{2}SCAN, but a material that is unstable by 3 meV/atom could (as was the case with *Pnma* $SnBr_2$ in Section II). Determining an appropriate threshold is necessary to properly target r^{2}SCAN calculations.

To inform this question, in Appendix A we evaluate the extent to which r^{2}SCAN changes the energy above hull of unstable polymorphs. Examining approximately 7300 unstable materials with a GGA+(U) energy above hull of 50 meV/atom or less, we find that in 95% of cases, the energy above hull either *increases* or decreases by no more than 19 meV/atom (see Figure A.1). This means that materials more than 19 meV/atom above the GGA(+U) hull would only be stabilized by r^{2}SCAN in rare cases. Hence, we adopt a threshold of 20 meV/atom as our definition of "close to the hull" for purposes of prioritizing calculations.

By way of comparison, we note that among 16 systems identified by Yang et al. [28] in which SCAN stabilized the correct ground state and GGA(+U) did not, the energies above hull of the experimental ground states in GGA(+U) ranged from 2 to 50 meV/atom. Another study showed that SCAN mispredicted the ground states of TiO_2 and FeS_2, with misprediction on the order of 50 meV/atom as well [39]. Thus, although based on analysis of a large set of materials, our selection of 20 meV/atom as a "safe" threshold is not guaranteed to capture the r^{2}SCAN ground state polymorph in every case. A higher threshold could certainly be chosen if greater confidence in capturing the correct ground states is required.

C. Failures of structure matching

In Section II A we established the need to obtain r^{2}SCAN energies of GGA(+U) ground states, which serve as reference energies for constructing mixed phase diagrams. To obtain the most accurate r^{2}SCAN energies, we generally perform r^{2}SCAN structure optimizations rather than single-point calculations and then use the PYMATGEN [36] `StructureMatcher` algorithm to determine whether the r^{2}SCAN-relaxed structure is the same (within tolerances) as the GGA(+U) starting structure.

In the vast majority of cases, the r^{2}SCAN-relaxed structure and the GGA(+U) starting structure match, allowing us to use the r^{2}SCAN energy as a reference energy. However in selected cases (some 1% of all materials we have computed thus far), r^{2}SCAN will optimize to a structure that is no longer considered equivalent to the starting structure. This is especially common for the crystal structures of diatomic molecules (e.g., H_2, Cl_2, O_2) in which the different treatment of short- and medium-range interactions by r^{2}SCAN compared to PBE is particularly significant.

We address this issue in two ways. In some cases, manual inspection of the structures allows us to establish that they represent the same material, and hence that the r^{2}SCAN energy can be used as a reference energy. However, manual inspection is not feasible for high-throughput work. Instead, we perform single-point calculations for any materials in which the r^{2}SCAN-relaxed structure no longer matches the input structure. The r^{2}SCAN single-point calculation is guaranteed to match the corresponding GGA(+U)-optimized structure and provides an r^{2}SCAN energy that can serve as a reference energy. Meanwhile, an r^{2}SCAN optimization of the same structure (which may no longer be the same according to the `StructureMatcher`) is guaranteed to have a similar or lower energy than the single point and will be added to the hull at the correct position by application of Rule #1. Performing r^{2}SCAN single points also provides a means of obtaining reference energies for large structures that would be impractical to optimize in r^{2}SCAN within reasonable computational limits (see Section III D).

D. Prioritizing r^{2}SCAN calculations for maximum benefit

We conclude our discussion of practical considerations by considering the best strategy for prioritizing r^{2}SCAN calculations, given that computational resources are limited and that its cost is still approximately 5× that of PBE [18].

We can define several levels of "calculation coverage" (meaning, subsets of materials that have all been recomputed with r^{2}SCAN, Figure 3) based on the mixing rules we have established. In order to apply Mixing Rule #1, at least two r^{2}SCAN optimizations at a single composition are needed: one for the GGA(+U) ground state and one for another polymorph. To apply Rule #2, we require r^{2}SCAN energies for every GGA(+U) ground state or (ideally) every GGA(+U) material within 20 meV/atom of the hull. These energies are preferably obtained from structure optimizations, although as discussed above, single-point calculations can be used, with the risk of a slightly less accurate hull shape. The pinnacle of calculation coverage (which may have less value that its computational cost, as noted in the Introduction) is full recomputation of all materials using r^{2}SCAN.

With a goal of achieving second- or third-level cov-

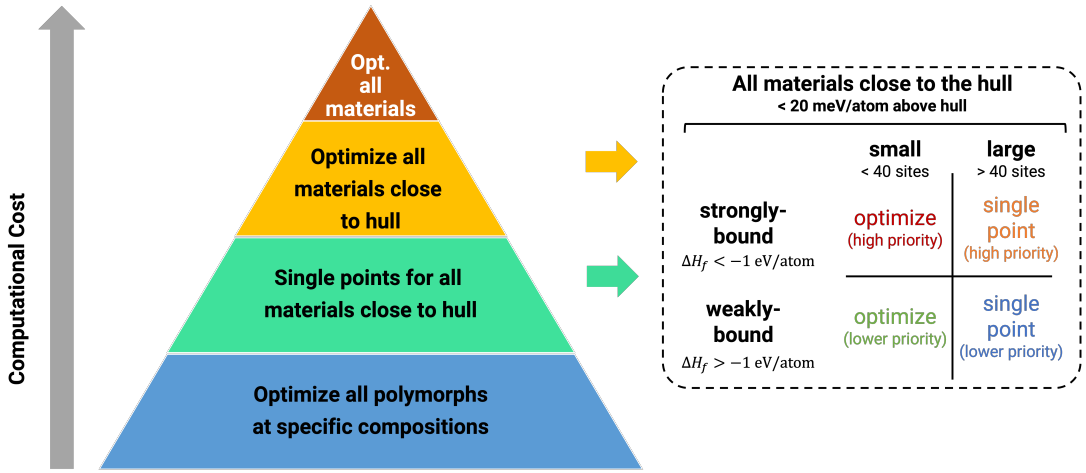

FIG. 3. Strategies for prioritizing higher level calculations in large materials databases. Left: different stages of calculation coverage. The first level enables application of Mixing Rule #1, while the second and third levels facilitate application of Rule #2. The fourth level (re-optimizing all materials with higher level calculations) is not necessary. Right: Methods used by the Materials Project to pursue second- and third-level coverage of r^{2}SCAN calculations. Optimizations of small, strongly-bound materials have the highest priority. Single-point calculations are used for large structures. Weakly-bound materials have lower priority. See Section III D for further details.

erage, we can identify several strategies for prioritizing which materials to calculate in order to maximize the benefits of the mixing scheme for formation energy prediction. To do so, we classify materials close to the hull as 1) strongly- or weakly-bound and 2) small or large.

Previous studies [18, 22] established that SCAN and r^{2}SCAN predict substantially more accurate formation energies than PBE or PBEsol for "strongly-bound" materials, i.e., materials whose GGA($+U$)-predicted formation energy is lower than -1 eV/atom. The improvement in accuracy for "weakly-bound" materials is more modest. As such, creating mixed phase diagrams for strongly-bound systems is likely to improve overall accuracy the most, and hence we assign higher priority to strongly-bound materials.

With respect to size, experience indicates that optimizations of large structures (e.g., larger than approximately 40 sites) with r^{2}SCAN will often exceed typical maximum wall time limits at supercomputing centers (e.g. 48 hr). This is not to say optimization is impossible; rather, in a high-throughput computing context it does not usually make sense to invest an excessive amount of computing nodes or wall time into a single material. As such, we choose to perform single-point calculations for large materials in order to obtain a reference energy (albeit a less accurate one) so that Rule #2 can be applied. Fully-optimized structures can be obtained as computational resources allow, and added into the mixed phase diagrams according to Rule #1.

IV. EXAMPLES

A. Application to a metastable ternary nitride system

As a practical example of our complete mixing scheme, we use it to investigate compound metastability in the ternary Zn–Sb–N system. Nitrides remain relatively unexplored compared to other chemical spaces, even though they exhibit the largest range of thermodynamically-accessible metastable states among inorganic materials [42, 43], which is thought to be a consequence of the large cohesive energy of metal-nitrogen bonds that kinetically traps metastable structures [40]. Compared to stable nitrides, metastable nitrides are more likely to contain metal cations in high oxidation states, which imparts unique semiconducting properties that make these materials interesting for electronic and photovoltaic applications, among others [29, 40, 43].

Metastable nitrides are relatively rare in nature and difficult to synthesize experimentally due to the high stability of molecular N_2. However, the use of reactive nitrogen precursors such as ammonia, azide compounds, or plasma-cracked atomic N allow nitrogen chemical potentials of up to +1 eV/N above the hull to be reached in laboratory synthesis [29, 40, 41]. Recent experimental studies [44–46] have reported synthesis of several metastable nitrides (Cu_3N, Sn_3N_4, and Ti-alloyed Sn_3N_4). Ternary Wurtzite-based nitrides, such as $MgSnN_2$, $ZnSnN_2$, $ZnGeN_2$, and $ZnSiN_2$, have received specific attention recently as potential alternatives to III-V semiconductors. [41, 44]. Computational screening studies [29, 40] recently predicted three new metastable ternary phases ($ZnSb_2N_4$, Zn_2SbN_3, and Zn_3SbN_3) and

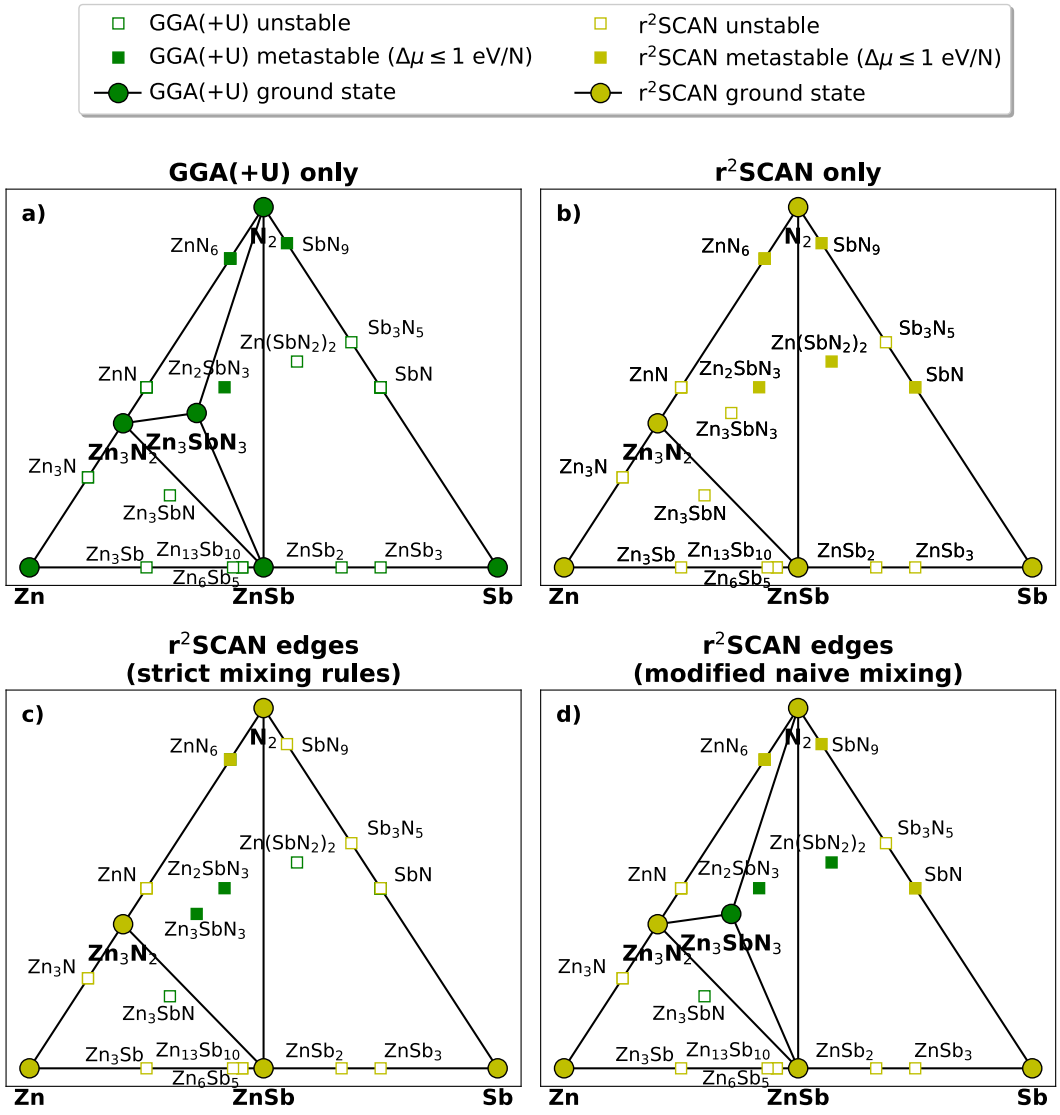

FIG. 4. Zn–Sb–N phase diagrams illustrating different mixing strategies for GGA($+U$) and r^{2}SCAN calculations. a) GGA($+U$) only; b) r^{2}SCAN only; c) strict application of Rule #1 and #2 to calculations comprising r^{2}SCAN energies for all elements and binary phases with GGA($+U$) energies for all ternary phases d) same set of calculations as c), but using modified naive mixing in which binary hulls are constructed from r^{2}SCAN formation energies. Phases labeled "metastable" are phases that can be stabilized by a +1 eV/N increase in the nitrogen chemical potential, which is achievable in laboratory synthesis [29, 40, 41]. Tabulated r^{2}SCAN and GGA($+U$) energies for all materials are provided in Appendix E.

a new metastable binary phase (SbN) in the Zn–Sb–N chemical space. Zn_2SbN_3, the first Sb-based nitride semiconductor ever reported, was experimentally realized [40, 41, 47] and exhibited promising electronic properties for photovoltaic and water splitting applications. SbN was predicted to be relatively close to the metastability limit (requiring +0.8 eV/N to stabilize) [29] and is the subject of ongoing investigations as another potential Sb-based nitride semiconductor.

Given the diverse bonding characteristics of nitrogen compounds, computational predictions of metastability can be particularly sensitive to the choice of functional and energy correction scheme (e.g., GGA vs. GGA+U vs. r^{2}SCAN). For example, Sun et al. [29] showed that for many binary nitride systems, PBE overstabilizes the nitrogen-rich region of the convex energy hull, while GGA+U overstabilized the nitrogen-poor region. SCAN was found to predict formation enthlapies with good accuracy across both portions of the hull [29]. To expand on this previous work and inform future high-throughput screening studies, we evaluate how the use of a mixed r^{2}SCAN / GGA($+U$) ternary phase diagram would affect these predictions.

Figures 4a and 4b show the phase diagrams computed entirely using GGA($+U$) and r^{2}SCAN calculations, respectively. Both the pure GGA($+U$) and pure r^{2}SCAN

phase diagrams predict that Zn_2SbN_3 and SbN are metastable, consistent with the previous studies. However, the energy above hull of both metastable compositions of interest is higher in r^{2}SCAN. r^{2}SCAN predicts 30 meV/atom above hull for Zn_2SbN_3 (vs. 20 meV/atom in GGA), reflecting the overstabilization of the N-rich region of the phase diagram in GGA($+U$) noted by Sun et al. [29]. r^{2}SCAN predicts 260 meV/atom above hull for SbN (vs. 172 meV/atom in GGA), but in the r^{2}SCAN diagram this material falls within the metastable synthesizability limit, consistent with experimental reports [29]. The other notable differences between the GGA($+U$) and r^{2}SCAN phase diagrams are that Zn_3SbN_3, which has not been synthesized to the best of our knowledge and is not in the ICSD, is predicted stable by GGA($+U$) but unstable by r^{2}SCAN, while $ZnSb_2N_4$ is unstable in GGA($+U$) but metastable in r^{2}SCAN. The stable / metastable / unstable classification for all other compositions is the same in both diagrams.

Moving to mixed phase diagrams, we now consider a situation in which only the elements and binary compositions have been computed with r^{2}SCAN, while all ternary phases remain in GGA($+U$). We compare two methods of constructing this mixed ternary phase diagram in Figures 4c and 4d. In Figure 4c, we apply Mixing Rule #1 and #2 strictly (i.e., considering the entire phase diagram at once). In this scenario, because we do not have a r^{2}SCAN calculation for the GGA($+U$) reference structure Zn_3SbN_3, *the hull is still calculated using GGA($+U$) energies* (with the exception of polymorphs stablized by r^{2}SCAN, as discussed later). r^{2}SCAN polymorphs for each element or binary composition are placed on this GGA($+U$) hull by anchoring to the respective reference states according to Rule #1.

Inspection of Figure 4c shows broad similarity to the pure r^{2}SCAN diagram (Figure 4b), with a few notable differences. Zn_3SbN_3 is predicated unstable in the pure r^{2}SCAN diagram yet metastable in the mixed diagram. For SbN the reverse is true: this material is predicted metastable in the pure r^{2}SCAN diagram but unstable in this mixed diagram. The convex energy hull in Figure 4c is constructed with GGA($+U$) energies, so it is identical to that of Figure 4a with one significant exception. As noted in Section II B, Rule #1 can cause the energy of the convex hull to decrease in cases where r^{2}SCAN stabilizes a different polymorph than GGA($+U$). In this case, r^{2}SCAN stabilizes a different structure for N_2 (which is a crystalline solid at 0 K) that is 1.8 meV/atom *lower* in energy than the reference energy (see Figure B.1), causing it to be placed below the GGA($+U$) hull and thereby "lowering" the hull energy of the N-rich region in the mixed phase diagram. This causes Zn_3SbN_3, which is predicted stable in the pure GGA($+U$) phase diagram, to move off the hull by 0.4 meV/atom and become metastable. The energy above hull for SbN increases by 1 meV/atom, and hence it retains its classification as unstable consistent with the GGA($+U$) phase diagram.

(Figure 4d) presents an alternative phase diagram constructed by fully applying Rules #1 and #2 to the binary edges and then adding GGA($+U$) energies for ternary phases by modified naive mixing, as discussed in Section III A. Here, the edges of the diagram are identical to those predicted by a pure r^{2}SCAN diagram because we have full coverage of all GGA($+U$) ground states and hence Rule #2 applies. In the interior of the diagram, three of the four ternary compositions retain the same stable/unstable/metastable classification they have in the pure r^{2}SCAN diagram, while Zn_3SbN_3 is predicted to be stable in the GGA($+U$) diagram (whereas it is predicted unstable in the pure r^{2}SCAN diagram).

As noted in Section III A, the modified form of naive mixing employed to construct Figure 4d is thermodynamically less consistent than strict application of Rule #1 and #2 (Figure 4c), and should only be invoked when *consistency between binary and higher dimension phase diagrams is essential.* In this example, where the metastability of phases is of primary interest, it would be advisable to apply the mixing rules strictly to ensure that the entire convex hull is constructed in a consistent manner. Indeed, among the two mixed diagrams, Figure 4c shows the most consistency with the pure r^{2}SCAN diagram.

B. Application to aqueous phase stability

Finally, we demonstrate how the mixing scheme presented here can be used to inform aqueous phase stability predictions. The computational Pourbaix diagram formalism of Persson et al. [35, 48] generates aqueous stability (pH-pE) diagrams by referencing experimental free energies of dissolved ions to DFT-predicted formation energies derived from solid phase diagrams. As such, the mixing scheme presented here can be applied to the creation of Pourbaix diagrams in addition to solid phase diagrams. SCAN-derived Pourbaix diagrams, for example, were shown to be systematically more accurate for transition metal oxides [49]. However, the large number of stable phases needed to build computational Pourbaix diagrams may preclude calculating entire chemical spaces in SCAN or r^{2}SCAN, motivating the usefulness of our mixing scheme in this context.

We illustrate the mixing scheme on the Se-O system, for which the PBE-derived Pourbaix diagram is known to be inaccurate with respect to experiment [49]. Specifically, it predicts a stable SeO_2 phase that is not observed experimentally (Figure 5a). Creating a computational Pourbaix diagram of this system requires a solid phase diagram of the Se–O–H chemical system, which contains 85 individual materials, according to the Materials Project database. Five of these materials contain more than 40 sites, and hence could be particularly challenging to recompute in r^{2}SCAN (see Section III D). Use of the mixing scheme allows us to construct the hull in r^{2}SCAN by performing calculations only for the ground states (9 materials) while retaining information from GGA($+U$)

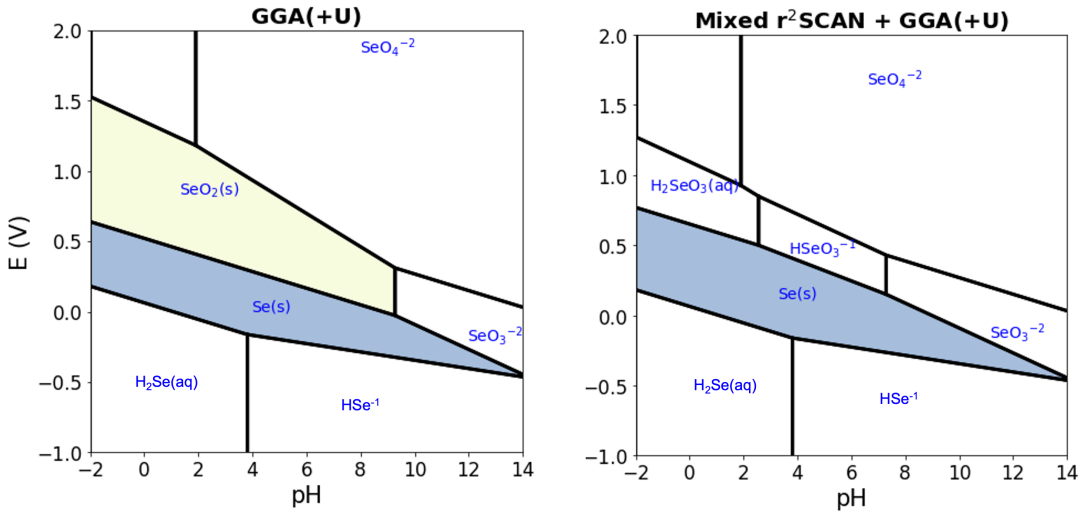

FIG. 5. Pourbaix diagram of Se–O constructed using GGA(+U) calculations (left) and the mixing scheme presented in this work (right) at a total Se concentration of 10^{-6} mol/L. Shaded regions predict stable solid phases. Tabulated r^{2}SCAN and GGA(+U) energies for all materials are provided in Appendix E.

about the metastability of other phases.

The resulting Pourbaix diagram built from mixed r^{2}SCAN and GGA(+U) energies (Figure 5b) correctly predicts that the oxide phase SeO_2 is unstable (unlike the pure GGA(+U) diagram), in agreement with Pourbaix diagrams presented by Wang et al. [49] that were prepared from both experimental data and pure SCAN calculations. Hence for this system, our mixing scheme has made it possible to leverage a relatively small number of calculations and achieve similar predictive accuracy as full recalculation of all materials with SCAN.

C. Summary

In summary, we have developed a mixing scheme to enable construction of phase diagrams that combine formation energies from any two DFT functionals. Such a capability is important to high-throughput materials screening efforts because it allows a relatively low-coverage, high-fidelity set of calculations (here, r^{2}SCAN) to be used in concert with existing high-coverage, lower-fidelity calculations (here, GGA(+U)) to improve the accuracy of phase stability predictions. Our scheme allows mixing r^{2}SCAN and GGA(+U) calculations when as few as two r^{2}SCAN calculations (one corresponding to a GGA(+U) ground state) are available, and scales smoothly to cases where entire binary, ternary, or higher-dimensional chemical systems are calculated in r^{2}SCAN. We identified specific guidelines that can be used to target limited computational resources towards materials where r^{2}SCAN calculations are likely to improve accuracy the most, and illustrated how the mixing scheme can be applied to solid and aqueous phase stability predictions.

V. METHODS

We employed the Vienna *ab initio* Simulation Package (VASP) [50, 51] v.6.1.1 in conjunction with v.54 of the projector-augmented wave (PAW) PBE pseudopotentials [52] for all r^{2}SCAN calculations in this work. We employed a two-step high-throughput workflow described elsewhere [18], which comprises a structure optimization with PBEsol [25] to generate a initial guess of the charge density, followed by a subsequent structure optimization with r^{2}SCAN [24]. These calculations were force-converged, with a plane-wave energy cutoff of 680 eV and a bandgap-dependent k-point density [18, 53], which were developed to achieve a formation energy converged to within approximately 1 meV/atom. We do not apply any energy corrections to the resulting r^{2}SCAN energies. For context regarding corrections, in Appendix D we fit energy corrections to diatomic gases and show that the corrections that would be applied to r^{2}SCAN are substantially smaller than those that have been widely used for GGA(+U) [14, 15].

PBE calculations were retrieved from the Materials Project REST API [54]. Calculations for transition metal oxides and fluorides contained a Hubbard U value and incorporated the GGA/GGA+U mixing scheme of Jain et al. [9], in addition to empirical corrections applied to some chemical systems [10]. We refer to these calculations as GGA(+U) throughout this work.

VI. DATA AVAILABILITY

All data referenced herein are publicly available in the Materials Project database [54]. At the time of this publication the database contains r^{2}SCAN calcula-

tions for approximately 33,000 materials, corresponding to 77% of all elements, binary, and ternary materials within 20 meV/atom of the GGA($+U$) convex energy hull. Our computational workflow has been implemented into the PYMATGEN [36] and ATOMATE [55] packages as of version 2020.1.28 and 0.9.5, respectively, for readers wishing to utilize it in their own work. The mixing scheme described herein is available in the MATERIALSPROJECTDFTMIXINGSCHEME class in PYMATGEN [36] as of release 2022.1.20.

VII. ACKNOWLEDGEMENTS

The authors gratefully acknowledge Stephan Lany (National Renewable Energy Laboratory) for contributing novel structures in the Zn–Sb–N system, Julia Yang (University of California, Berkeley) for contributing the $SnBr_2$ structures, and Matthew McDermott (University of California, Berkeley) for helpful discussions regarding construction of phase diagrams with a shifted nitrogen chemical potential.

This work was intellectually led by the Materials Project, which is funded by the U.S. Department of Energy, Office of Science, Office of Basic Energy Sciences, Materials Sciences and Engineering Division, under Contract no. DE-AC02-05-CH11231: Materials Project program KC23MP. Additional support was also provided by the Data Infrastructure Building Blocks (DIBBS) Local Spectroscopy Data Infrastructure (LSDI) project funded by the National Science Foundation (NSF) under Award Number 1640899. A.S.R. acknowledges support via a Miller Research Fellowship from the Miller Institute for Basic Research in Science, University of California, Berkeley.

VIII. AUTHOR CONTRIBUTIONS

Ryan Kingsbury: Conceptualization, Software, Methodology, Data Curation, Formal Analysis, Visualization, Validation, Writing - Original Draft, Writing - Review & Editing. Andrew S. Rosen: Data Curation, Visualization, Formal Analysis, Validation, Writing - Original Draft, Writing - Review & Editing. Ayush Gupta: Formal Analysis, Visualization. Jason Munro: Software, Data Curation, Validation. Shyue Ping Ong: Methodology, Writing - Review & Editing. Anubhav Jain: Methodology, Writing - Review & Editing. Shyam Dwaraknath: Conceptualization, Methodology, Writing - Review & Editing, Supervision. Matthew Horton: Conceptualization, Methodology, Writing - Review & Editing, Supervision. Kristin Persson: Conceptualization, Methodology, Writing - Review & Editing, Supervision, Funding Acquisition, Project Administration.

IX. COMPETING INTEREST STATEMENT

The authors declare no competing financial interests.

X. REFERENCES

[1] A. Jain, S. P. Ong, G. Hautier, W. Chen, W. D. Richards, S. Dacek, S. Cholia, D. Gunter, D. Skinner, G. Ceder, and K. A. Persson, The Materials Project: A materials genome approach to accelerating materials innovation, APL Materials **1**, 011002 (2013).

[2] S. Curtarolo, W. Setyawan, S. Wang, J. Xue, K. Yang, R. H. Taylor, L. J. Nelson, G. L. Hart, S. Sanvito, M. Buongiorno-Nardelli, N. Mingo, and O. Levy, Aflowlib.org: A distributed materials properties repository from high-throughput ab initio calculations, Computational Materials Science **58**, 227 (2012).

[3] J. E. Saal, S. Kirklin, M. Aykol, B. Meredig, and C. Wolverton, Materials design and discovery with high-throughput density functional theory: The open quantum materials database (oqmd), JOM **65**, 1501 (2013).

[4] S. Kirklin, J. E. Saal, B. Meredig, A. Thompson, J. W. Doak, M. Aykol, S. Rühl, and C. Wolverton, The Open Quantum Materials Database (OQMD): Assessing the accuracy of DFT formation energies, npj Computational Materials **1**, 10.1038/npjcompumats.2015.10 (2015).

[5] K. Choudhary, K. F. Garrity, A. C. Reid, B. DeCost, A. J. Biacchi, A. R. H. Walker, Z. Trautt, J. Hattrick-Simpers, A. G. Kusne, A. Centrone, A. Davydov, J. Jiang, R. Pachter, G. Cheon, E. Reed, A. Agrawal, X. Qian, V. Sharma, H. Zhuang, S. V. Kalinin, B. G. Sumpter, G. Pilania, P. Acar, S. Mandal, K. Haule, D. Vanderbilt, K. Rabe, and F. Tavazza, The joint automated repository for various integrated simulations (jarvis) for data-driven materials design, npj Computational Materials **6**, 1 (2020).

[6] L. Himanen, A. Geurts, A. S. Foster, and P. Rinke, Data-driven materials science: Status, challenges, and perspectives, Advanced Science **6**, 1900808 (2019).

[7] J. P. Perdew, K. Burke, and M. Ernzerhof, Generalized gradient approximation made simple, Phys. Rev. Lett. **77**, 3865 (1996).

[8] D. C. Langreth and J. P. Perdew, Theory of nonuniform electronic systems. i. analysis of the gradient approximation and a generalization that works, Physical Review B 10.1103/PhysRevB.21.5469 (1980).

[9] A. Jain, G. Hautier, S. P. Ong, C. J. Moore, C. C. Fischer, K. A. Persson, and G. Ceder, Formation enthalpies by mixing GGA and GGA+U calculations, Physical Review B - Condensed Matter and Materials Physics **84**, 1 (2011).

[10] A. Wang, R. Kingsbury, M. McDermott, M. Horton, A. Jain, S. P. Ong, S. Dwaraknath, and K. A. Persson, A framework for quantifying uncertainty in DFT energy

corrections, Scientific Reports **11**, 10.1038/s41598-021-94550-5 (2021).
[11] C. Chen, Y. Zuo, W. Ye, X. Li, Z. Deng, and S. P. Ong, A critical review of machine learning of energy materials, Advanced Energy Materials **10**, 1903242 (2020).
[12] P. Mori-Sánchez, A. J. Cohen, and W. Yang, Many-electron self-interaction error in approximate density functionals, The Journal of chemical physics **125**, 201102 (2006).
[13] J. P. Perdew, Climbing the ladder of density functional approximations, MRS Bulletin **38**, 743 (2013).
[14] S. Grindy, B. Meredig, S. Kirklin, J. E. Saal, and C. Wolverton, Approaching chemical accuracy with density functional calculations: Diatomic energy corrections, Physical Review B - Condensed Matter and Materials Physics **87**, 1 (2013).
[15] L. Wang, T. Maxisch, and G. Ceder, Oxidation energies of transition metal oxides within the GGA+U framework, Physical Review B - Condensed Matter and Materials Physics **73**, 1 (2006).
[16] V. I. Anisimov, J. Zaanen, and O. K. Andersen, Band theory and mott insulators: Hubbard u instead of stoner i, Phys. Rev. B **44**, 943 (1991).
[17] S. Grimme, A. Hansen, J. G. Brandenburg, and C. Bannwarth, Dispersion-Corrected Mean-Field Electronic Structure Methods, Chemical Reviews **116**, 5105 (2016).
[18] R. Kingsbury, A. Gupta, C. Bartel, J. Munro, S. Dwaraknath, M. Horton, and K. Persson, Performance comparison of r2scan and scan metagga density functionals for solid materials via an automated, high-throughput computational workflow, ChemRxiv 10.33774/chemrxiv-2021-gwm9m-v2 (2021).
[19] S. Lany, Semiconductor thermochemistry in density functional calculations, Physical Review B - Condensed Matter and Materials Physics **78**, 1 (2008).
[20] M. Aykol and C. Wolverton, Local environment dependent GGA+U method for accurate thermochemistry of transition metal compounds, Physical Review B - Condensed Matter and Materials Physics **90**, 1 (2014).
[21] R. Friedrich, D. Usanmaz, C. Oses, A. Supka, M. Fornari, M. Buongiorno Nardelli, C. Toher, and S. Curtarolo, Coordination corrected ab initio formation enthalpies, npj Computational Materials **5**, 1 (2019), arXiv:arXiv:1811.08952v2.
[22] E. B. Isaacs and C. Wolverton, Performance of the strongly constrained and appropriately normed density functional for solid-state materials, Physical Review Materials **2**, 1 (2018).
[23] G. Hautier, S. P. Ong, A. Jain, C. J. Moore, and G. Ceder, Accuracy of density functional theory in predicting formation energies of ternary oxides from binary oxides and its implication on phase stability, Phys. Rev. B **85**, 155208 (2012).
[24] J. W. Furness, A. D. Kaplan, J. Ning, J. P. Perdew, and J. Sun, Accurate and numerically efficient r2scan meta-generalized gradient approximation, The Journal of Physical Chemistry Letters **11**, 8208 (2020).
[25] J. P. Perdew, A. Ruzsinszky, G. I. Csonka, O. A. Vydrov, G. E. Scuseria, L. A. Constantin, X. Zhou, and K. Burke, Restoring the density-gradient expansion for exchange in solids and surfaces, Phys. Rev. Lett. **100**, 136406 (2008).
[26] J. Sun, A. Ruzsinszky, and J. Perdew, Strongly Constrained and Appropriately Normed Semilocal Density Functional, Physical Review Letters **115**, 1 (2015).
[27] Y. Zhang, D. A. Kitchaev, J. Yang, T. Chen, S. T. Dacek, R. A. Sarmiento-Pérez, M. A. Marques, H. Peng, G. Ceder, J. P. Perdew, and J. Sun, Efficient first-principles prediction of solid stability: Towards chemical accuracy, npj Computational Materials **4**, 10.1038/s41524-018-0065-z (2018).
[28] J. H. Yang, D. A. Kitchaev, and G. Ceder, Rationalizing accurate structure prediction in the meta-GGA SCAN functional, Physical Review B **100**, 035132 (2019).
[29] W. Sun, A. Holder, B. Orvañanos, E. Arca, A. Zakutayev, S. Lany, and G. Ceder, Thermodynamic Routes to Novel Metastable Nitrogen-Rich Nitrides, Chemistry of Materials **29**, 6936 (2017).
[30] J.-S. Park, Comparison study of exchange-correlation functionals on prediction of ground states and structural properties, Current Applied Physics **22**, 61 (2021).
[31] C. J. Bartel, A. W. Weimer, S. Lany, C. B. Musgrave, and A. M. Holder, The role of decomposition reactions in assessing first-principles predictions of solid stability, npj Computational Materials **5**, 10.1038/s41524-018-0143-2 (2019).
[32] D. Mejia-Rodriguez and S. B. Trickey, Deorbitalized meta-GGA exchange-correlation functionals in solids, Physical Review B **98**, 10.1103/physrevb.98.115161 (2018).
[33] V. Stevanovic, S. Lany, X. Zhang, and A. Zunger, Correcting density functional theory for accurate predictions of compound enthalpies of formation: Fitted elemental-phase reference energies, Physical Review B - Condensed Matter and Materials Physics **85**, 1 (2012).
[34] See https://docs.materialsproject.org/methodology/gga-plus-u/.
[35] K. A. Persson, B. Waldwick, P. Lazic, and G. Ceder, Prediction of solid-aqueous equilibria: Scheme to combine first-principles calculations of solids with experimental aqueous states, Phys. Rev. B **85**, 235438 (2012).
[36] S. P. Ong, W. D. Richards, A. Jain, G. Hautier, M. Kocher, S. Cholia, D. Gunter, V. L. Chevrier, K. A. Persson, and G. Ceder, Python Materials Genomics (pymatgen): A robust, open-source python library for materials analysis, Computational Materials Science **68**, 314 (2013).
[37] T. R. Brumleve, Preparation, vapor pressure and thermochemistry of tin(II) bromide, ECS Proceedings Volumes **1992-16**, 50 (1992).
[38] I. Levin, Nist inorganic crystal structure database (icsd) (2020).
[39] B. Patra, S. Jana, L. A. Constantin, and P. Samal, Correct structural phase stability of FeS2, TiO2, and MnO2 from a semilocal density functional, The Journal of Physical Chemistry C **125**, 4284 (2021).
[40] W. Sun, C. J. Bartel, E. Arca, S. R. Bauers, B. Matthews, B. Orvananos, B.-R. Chen, M. F. Toney, L. T. Schelhas, W. Tumas, J. Tate, A. Zakutayev, S. Lany, A. M. Holder, and G. Ceder, A map of the inorganic ternary metal nitrides, Nature Materials **18**, 732 (2019).
[41] E. Arca, J. D. Perkins, S. Lany, A. Mis, B. R. Chen, P. Dippo, J. L. Partridge, W. Sun, A. Holder, A. C. Tamboli, M. F. Toney, L. T. Schelhas, G. Ceder, W. Tumas, G. Teeter, and A. Zakutayev, Zn2sbn3: Growth and characterization of a metastable photoactive semiconductor, Materials Horizons **6**, 1669 (2019).

[42] W. Sun, S. T. Dacek, S. P. Ong, G. Hautier, A. Jain, W. D. Richards, A. C. Gamst, K. A. Persson, and G. Ceder, The thermodynamic scale of inorganic crystalline metastability, Science Advances **2**, 10.1126/sciadv.1600225 (2016).

[43] A. L. Greenaway, C. L. Melamed, M. B. Tellekamp, R. Woods-Robinson, E. S. Toberer, J. R. Neilson, and A. C. Tamboli, Ternary nitride materials: Fundamentals and emerging device applications, Annual Review of Materials Research **51**, 591 (2021).

[44] A. L. Greenaway, A. Loutris, K. N. Heinselman, C. L. Melamed, R. R. Schnepf, M. B. Tellekamp, R. Woods-Robinson, R. Sherbondy, D. J. Bardgett, S. R. Bauers, A. Zakutayev, S. T. Christensen, S. Lany, and A. Tamboli, Combinatorial synthesis of magnesium tin nitride semiconductors, Journal of the American Chemical Society **142**, 8421 (2021), pMID: 32279492, https://doi.org/10.1021/jacs.0c02092.

[45] C. M. Caskey, R. M. Richards, D. S. Ginley, and A. Zakutayev, Thin film synthesis and properties of copper nitride, a metastable semiconductor, Mater. Horiz. **1**, 424 (2014).

[46] C. M. Caskey, J. A. Seabold, V. Stevanović, M. Ma, W. A. Smith, D. S. Ginley, N. R. Neale, R. M. Richards, S. Lany, and A. Zakutayev, Semiconducting properties of spinel tin nitride and other IV3n4 polymorphs, Journal of Materials Chemistry C **3**, 1389 (2015).

[47] A. Mis, S. Lany, G. L. Brennecka, and A. Tamboli, Exploring the phase space of zn2sbn3, a novel semiconducting nitride, Journal of Materials Chemistry C **9**, 13904 (2021).

[48] A. M. Patel, J. K. Nørskov, K. A. Persson, and J. H. Montoya, Efficient pourbaix diagrams of many-element compounds, Physical Chemistry Chemical Physics **21**, 25323 (2019).

[49] Z. Wang, X. Guo, J. Montoya, and J. K. Nørskov, Predicting aqueous stability of solid with computed pourbaix diagram using SCAN functional, npj Computational Materials **6**, 10.1038/s41524-020-00430-3 (2020).

[50] G. Kresse and J. Furthmüller, Efficiency of ab-initio total energy calculations for metals and semiconductors using a plane-wave basis set, Computational Materials Science **6**, 15 (1996).

[51] G. Kresse and J. Furthmüller, Efficient iterative schemes for ab initio total-energy calculations using a plane-wave basis set, Phys. Rev. B **54**, 11169 (1996).

[52] P. E. Blöchl, Projector augmented-wave method, Phys. Rev. B **50**, 17953 (1994).

[53] P. Wisesa, K. A. McGill, and T. Mueller, Efficient generation of generalized Monkhorst-Pack grids through the use of informatics, Physical Review B **93**, 1 (2016).

[54] S. P. Ong, S. Cholia, A. Jain, M. Brafman, D. Gunter, G. Ceder, and K. A. Persson, The materials application programming interface (API): A simple, flexible and efficient API for materials data based on REpresentational state transfer (REST) principles, Computational Materials Science **97**, 209 (2015).

[55] K. Mathew, J. H. Montoya, A. Faghaninia, S. Dwarakanath, M. Aykol, H. Tang, I. heng Chu, T. Smidt, B. Bocklund, M. Horton, J. Dagdelen, B. Wood, Z.-K. Liu, J. Neaton, S. P. Ong, K. Persson, and A. Jain, Atomate: A high-level interface to generate, execute, and analyze computational materials science workflows, Computational Materials Science **139**, 140 (2017).

[56] L. Ward, A. Dunn, A. Faghaninia, N. E. Zimmermann, S. Bajaj, Q. Wang, J. Montoya, J. Chen, K. Bystrom, M. Dylla, K. Chard, M. Asta, K. A. Persson, G. J. Snyder, I. Foster, and A. Jain, Matminer: An open source toolkit for materials data mining, Computational Materials Science **152**, 60 (2018).

XI. APPENDICES

Appendix A: Comparing the relative stability of polymorphs

The tendency of r^{2}SCAN to stabilize unstable polymorphs is of particular interest. In this section, we assess the extent to which r^{2}SCAN changes the energy above hull of polymorphs that are predicted to be unstable with GGA(+U), specifically focusing on structures with 0 meV/atom $< \Delta E_{\text{hull}}^{\text{GGA}(+U)} <$ 50 meV/atom. We define the parameter $\Delta\Delta E_{\text{hull}}^{\text{GGA}(+U)\rightarrow\text{r}^2\text{SCAN}}$, which is the change in the energy above hull of the GGA(+U) polymorph when going from GGA(+U) to r^{2}SCAN. Thus, if the structure is predicted to be unstable by GGA(+U) and moved closer to the hull with r^{2}SCAN, its $\Delta\Delta E_{\text{hull}}^{\text{GGA}(+U)\rightarrow\text{r}^2\text{SCAN}}$ will be negative (and vice versa).

The results of this analysis are shown in Figure A.1. In the majority of cases, the change in ΔE_{hull} is small (within a few meV/atom). We note that for 95% of the unstable GGA(+U) compounds within 50 meV/atom of the GGA(+U) hull, $\Delta\Delta E_{\text{hull}}^{\text{GGA}(+U)\rightarrow\text{r}^2\text{SCAN}}$ was greater than –19 meV/atom, and for 99% this value is –36 meV/atom. This means that compounds that are more than 19 meV/atom above the GGA(+U) hull are unlikely to appear on the r^{2}SCAN hull, while compounds more than 36 meV/atom above hull will only be stabilized by r^{2}SCAN in especially rare circumstances.

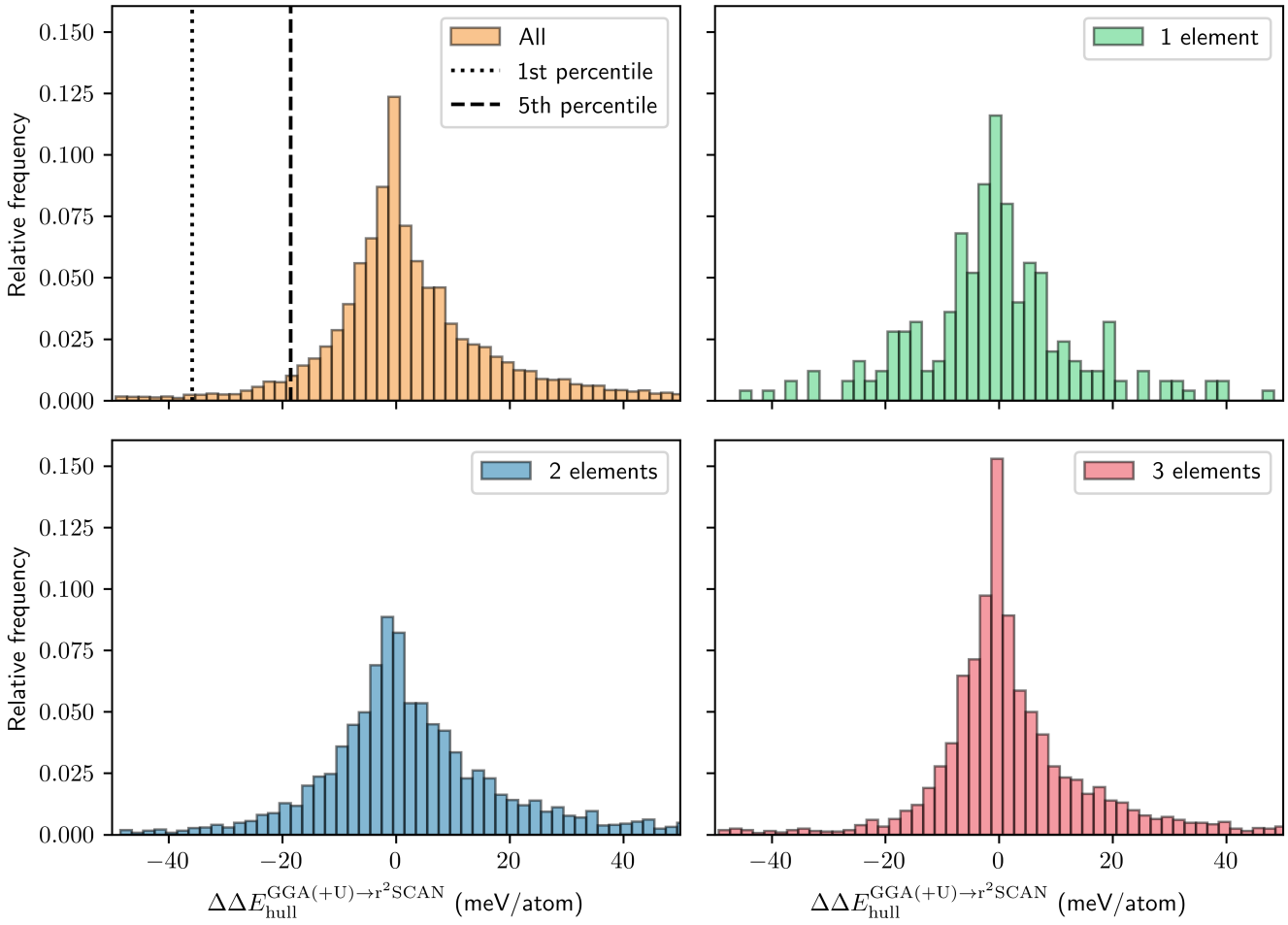

FIG. A.1. Change in energy above hull for polymorphs when going from GGA(+U) to r^{2}SCAN, $\Delta\Delta E_{\text{hull}}^{\text{GGA}(+U)\rightarrow\text{r}^2\text{SCAN}}$. Only polymorphs that are unstable in GGA(+U) and within 50 meV/atom of the GGA(+U) hull are included. The data is broken down by the number of unique elements in the considered structures.

Appendix B: Differences in elemental ground-state structures and energies

Here, we assess the frequency and magnitude with which r^{2}SCAN changes the relative stability of elemental structures compared to GGA, which we define as the change in the energy above hull for a given structure when going from GGA to r^{2}SCAN: $\Delta\Delta E_{\text{hull}}^{\text{GGA}\rightarrow\text{r}^2\text{SCAN}} \equiv \Delta E_{\text{hull}}^{\text{r}^2\text{SCAN}} - \Delta E_{\text{hull}}^{\text{GGA}}$. If r^{2}SCAN yields the same elemental ground-state structure as GGA, then $\Delta\Delta E_{\text{hull}}^{\text{GGA}\rightarrow\text{r}^2\text{SCAN}} = 0$ by definition. If GGA predicts elemental structure A to be 2 meV/atom higher in energy compared to stable elemental structure B, but r^{2}SCAN predicts elemental structure A to be stable and 2 meV/atom lower in energy than elemental structure B, then $\Delta\Delta E_{\text{hull}}^{\text{GGA}\rightarrow\text{r}^2\text{SCAN}} = -4$ meV/atom. Note that because all structures considered in this section are elemental, no U value is applied in this analysis.

Figure B.1 highlights the elements that have different ground-state structures between GGA and r^{2}SCAN as well as the magnitude of this energy difference, where applicable. Based on the results in Figure B.1, even for the elements where r^{2}SCAN stabilizes a different ground-state structure, the energy difference is often relatively small; the average value of $\Delta\Delta E_{\text{hull}}^{\text{GGA}\rightarrow\text{r}^2\text{SCAN}}$ is –30 meV/atom (or –12 meV/atom if including the 0 meV/atom change in energy above hull for the elements that do not have a different ground state). One pronounced exception is elemental Ce, for which the r^{2}SCAN ground state structure is unstable in GGA by 2 meV/atom, but the GGA ground state structure is unstable in r^{2}SCAN by 223 meV/atom. It should also be noted that, for some elements (i.e. Eu, Pu, Xe), r^{2}SCAN does not a yield a DFT-optimized structure that matches the GGA ground-state structure (as determined by the PYMATGEN [36] `StructureMatcher` algorithm and subsequent manual inspection). This is likely due in part to an improved treatment of van der Waals interactions with r^{2}SCAN.

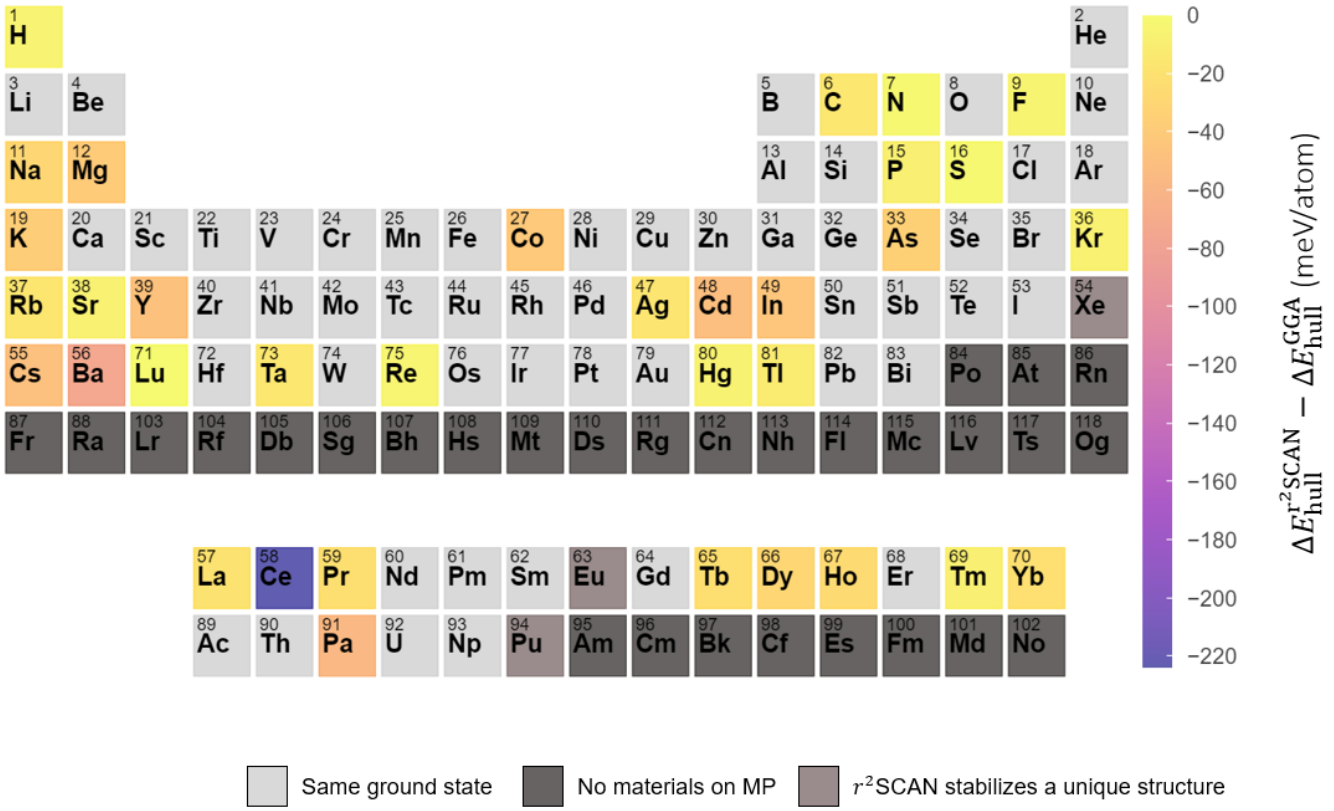

FIG. B.1. Energy differences in elemental ground-state structures computed with r^{2}SCAN and GGA. The color bar indicates the amount by which the energy above hull of the unstable polymorph changed with r^{2}SCAN compared to GGA. The elements shown as light gray have the same ground-state structure in both functionals. The elements shown as dark gray (i.e Po–Og)do not have entries on the Materials Project. The elements shown in brown (i.e. Xe, Eu, Pu) have have an r^{2}SCAN ground state that that was different from the GGA ground state (and also different from all other GGA polymorphs). All elements were calculated without a U value.

Appendix C: Accuracy of r^{2}SCAN-edged ternary phase diagrams

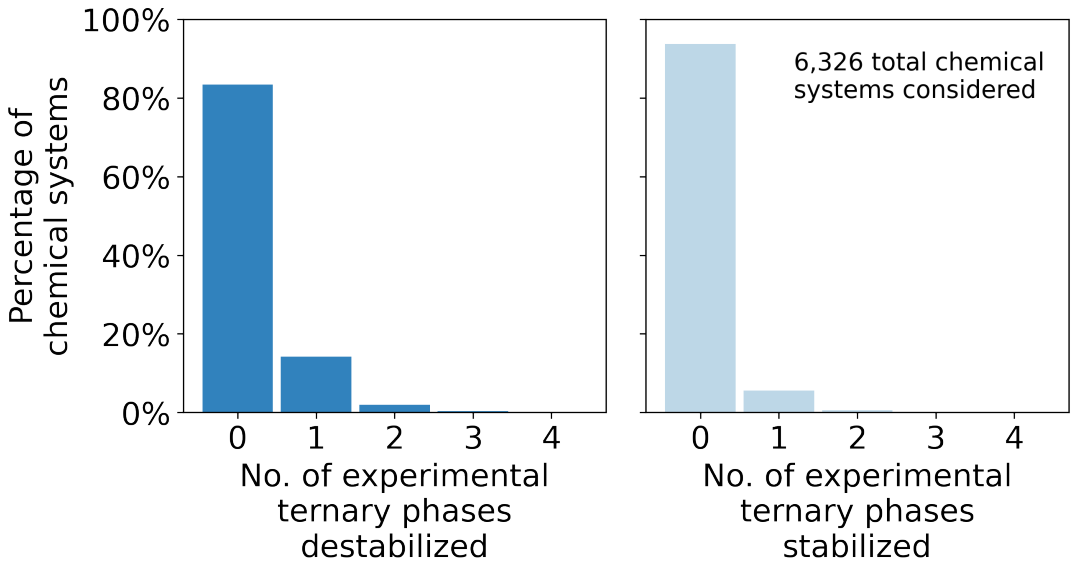

FIG. C.1. Changes to ternary phase stability predictions when constructing the hull using modified naive mixing as described in Section III A of the main text compared to pure GGA($+U$) for 6,326 ternary chemical systems. Left: number of experimental ternary phases predicted stable by pure GGA($+U$) that become unstable in the mixed diagram. Right: number of experimental ternary phases predicted unstable by pure GGA($+U$) that become stable in the mixed diagram. Experimental phases are phases that match one or more structures reported in the Inorganic Crystal Structure Database [38].

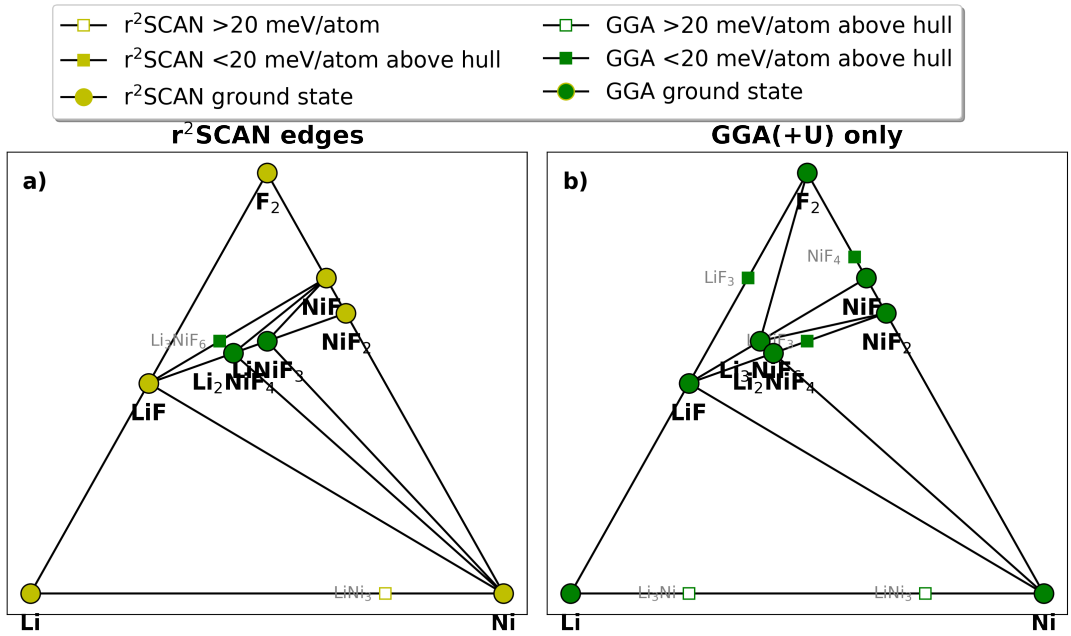

FIG. C.2. Example ternary phase diagram for the F–Li–Ni chemical system constructed by modified naive mixing as described in Section III A of the main text (left) and in pure GGA($+U$) (right). In the mixed diagram, the formation energies of all binary GGA($+U$) stable phases are replaced with r^{2}SCAN values. Some unstable binary GGA($+U$) phases are not shown. In the mixed diagram in this example, one stable ternary GGA($+U$) phase is destabilized and one unstable ternary phase is stabilized.

Appendix D: Diatomic energy corrections

One commonly used approach to addressing systematic errors in GGA functionals and improving the accuracy of DFT-predicted formation energies is to fit composition-dependent energy corrections to elements whose ground states are diatomic gases [14]. To evaluate the need for such corrections with meta-GGA calculations, we fit corrections to our r^{2}SCAN energies following the same procedure and set of experimental compounds as Grindy et al [14]. r^{2}SCAN and GGA($+U$) energies were derived using the methods described in Section V, except that all energy corrections were removed from GGA($+U$) energies prior to fitting. Experimental energies were obtained from the `expt_formation_enthalpy_kingsbury` dataset distributed with MATMINER [56], which is described further in Wang et al. and Kingsbury et al [10, 18].

The fitted corrections are summarized in Table D.1 and Figures D.1–D.5. Table D.1 also contains corrections fitted to GGA($+U$) energies in this work and the corrections obtained by Grindy et al. [14] for comparison. r^{2}SCAN corrections are substantially smaller than the corresponding GGA($+U$) corrections in all cases. For example, the energy correction for O_2 is -0.351 eV/O_2 for r^{2}SCAN, vs. -1.286 eV/O_2 when using GGA($+U$) energies. The improvement in the accuracy of nitride formation energies is particularly notable (see Fig. D.2). Here, the correction is reduced from 0.811 eV/N_2 with GGA($+U$) energies to just 0.055 eV/N_2 with r^{2}SCAN.

Given the small magnitude of the r^{2}SCAN energy corrections obtained here and considering that such corrections are inherently biased to simple chemistries by the nature of the fitting process, we elected not to apply any energy corrections and to use r^{2}SCAN energies as-is when constructing phase diagrams. For detailed study of specific chemical systems (e.g. chlorides or oxides), modest improvements in the accuracy of formation energies might be obtained by applying the corrections shown here.

TABLE D.1. Diatomic energy corrections to r^{2}SCAN formation energies (eV/X_2 molecule)

Molecule	r^{2}SCAN	MP GGA($+U$)	Grindy et al. [14]
O_2	-0.351	-1.286	-1.198
N_2	-0.055	-0.811	-0.892
H_2	-0.017	-0.312	-0.284
F_2	-0.165	-1.010	-0.884
Cl_2	-0.374	-1.105	-0.966

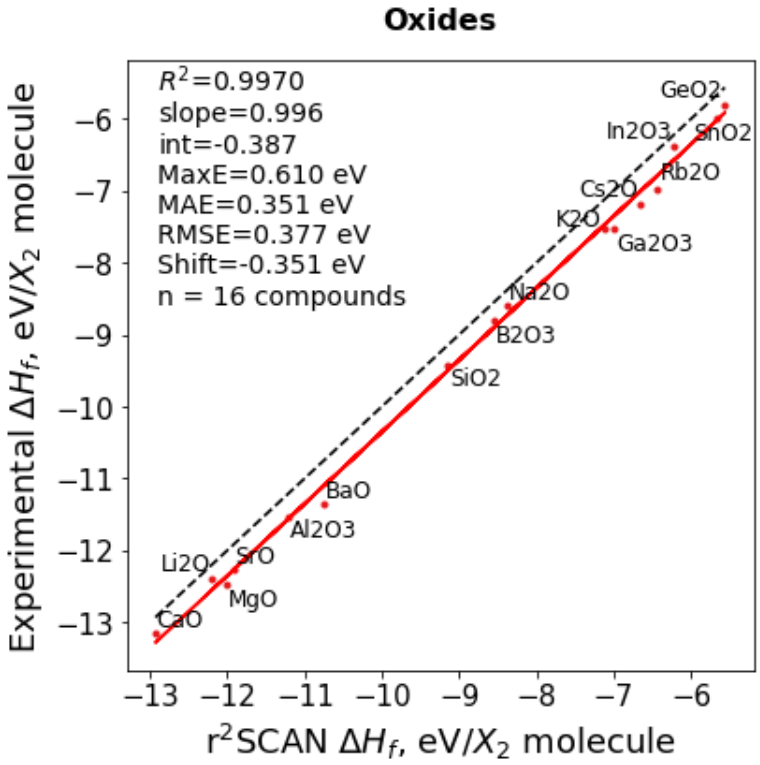

FIG. D.1. Experimental and r^{2}SCAN-computed ΔH_f for oxide compounds. The compounds correspond to those selected by Grindy et al. [14].

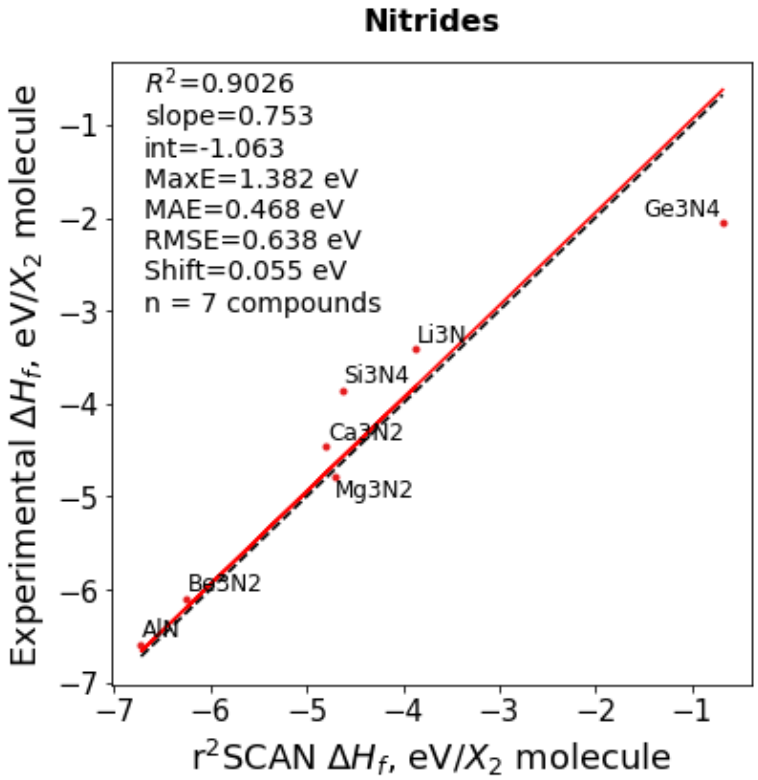

FIG. D.2. Experimental and r^{2}SCAN-computed ΔH_f for nitride compounds. The compounds correspond to those selected by Grindy et al. [14].

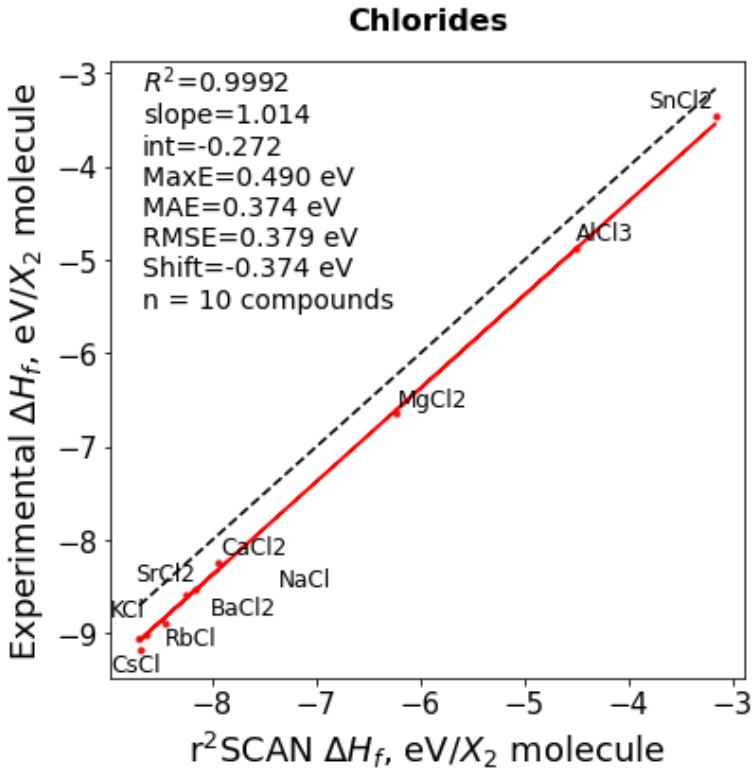

FIG. D.3. Experimental and r^{2}SCAN-computed ΔH_f for chloride compounds. The compounds correspond to those selected by Grindy et al. [14].

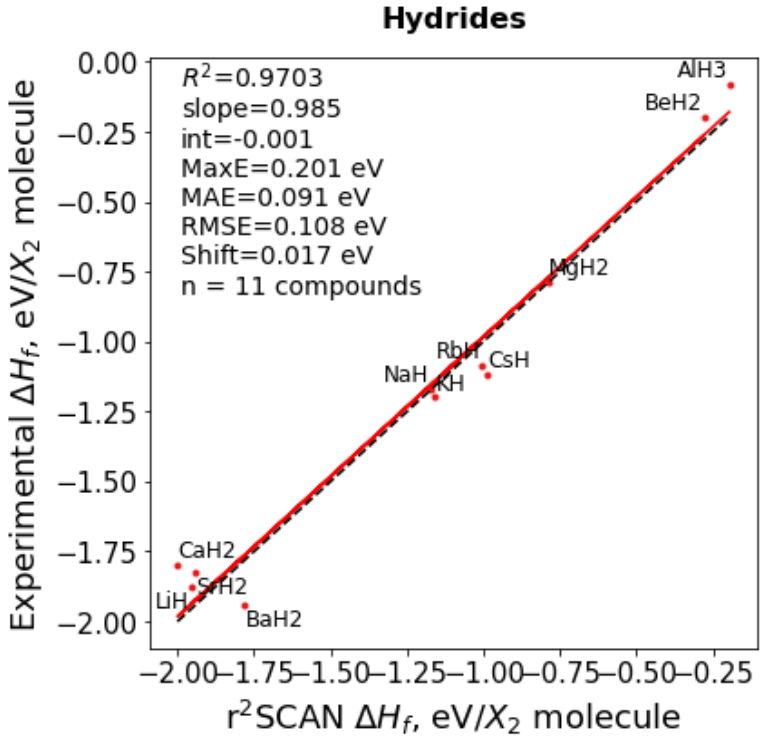

FIG. D.4. Experimental and r^{2}SCAN-computed ΔH_f for hydride compounds. The compounds correspond to those selected by Grindy et al. [14].

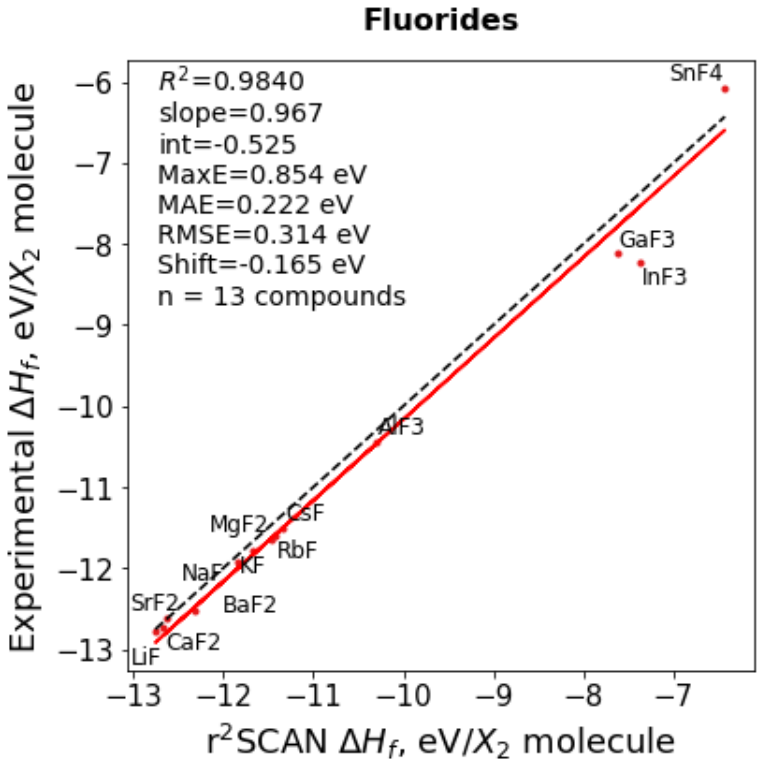

FIG. D.5. Experimental and r^{2}SCAN-computed ΔH_f for fluoride compounds. The compounds correspond to those selected by Grindy et al. [14].

Appendix E: Description of tabulated data files

Comma-separated value (.csv) files containing the composition, spacegroup, GGA(+U) and r^{2}SCAN energies of all materials used to construct the phase diagrams presented in the main text are included with the manuscript as Supporting Information. Each material (i.e., each distinct structure) is listed on a single row, with columns containing data from the corresponding GGA(+U) and/or r^{2}SCAN calculations. Some columns may be blank if, for example, one of the calculations was not performed or the r^{2}SCAN-relaxed structure did not match the GGA(+U)-relaxed structure. The data are organized into the following columns:

- `formula`: The reduced formula of the material.
- `spacegroup`: The spacegroup of the material's structure.
- `num_sites`: The number of atoms in the material's structure.
- `is_stable_1`: Boolean value indicating whether the material is stable on the GGA(+U) energy hull.
- `entry_id_1`: A unique identifier for the GGA(+U) calculation, if one is present. The identifier comprises the material ID (MP-ID) of the material in the Materials Project database with the type of calculation (either "GGA(+U)" or "R2SCAN") appended.
- `entry_id_2`: A unique identifier for the r^{2}SCAN calculation, if one is present. The identifier comprises the material ID (MP-ID) of the material in the Materials Project database with the type of calculation (either "GGA(+U)" or "R2SCAN") appended.
- `run_type_1`: The calculation type of `entry_id_1` (always "GGA(+U)" in this work).
- `run_type_2`: The calculation type of `entry_id_2` (always "R2SCAN" in this work).
- `energy_1`: The electronic energy (i.e., DFT energy) of the GGA(+U) calculation, in eV/atom.
- `energy_2`: The electronic energy (i.e., DFT energy) of the r^{2}SCAN calculation, in eV/atom.
- `hull_energy_1`: The energy of the GGA(+U) convex hull at this material's composition, in eV/atom.
- `hull_energy_2`: The energy of the r^{2}SCAN convex hull at this material's composition, in eV/atom.